2011 American Control Conference
on O'Farrell Street, San Francisco, CA, USA
June 29 - July 01, 2011

Optimal On-Off Controller with Charge Recovery for Thin-Film Piezoelectric Actuators for an Autonomous Mobile Micro-Robot

Biju Edamana, and Kenn Oldham, *Member, ASME*

***Abstract*— In this paper an efficient control strategy using charge recovery for a MEMS piezoelectric actuator is described. For piezoelectric actuators or other actuation schemes which act as capacitor loads, energy consumption can be reduced by minimizing the number of times the actuator is charged and by recovering the drained energy when it is turned off. An integer programming-based algorithm is used to drive micro-robotic legs consisting of piezoelectric actuators to a certain specific angle in a given time with the use of minimum energy. Partial charge recovery, which recovers a portion of the drained energy, is incorporated by making use of a lighter inductor. This allows the use of a more flexible controller than a pure ultra low-power on-off controller, with two or more intermediate voltage levels between the minimum and maximum voltages available to improve positioning accuracy, while also reducing energy consumption.**

I. Introduction

Recent developments in the area of Micro-Electromechanical System (MEMS) actuators have opened up opportunities to develop extremely small autonomous devices such as mobile micro-robots. In order to fulfil the potential of these devices they should carry their own power source. This poses the challenge of miniaturization of the energy source and its associated power electronics circuitry as well as a strict constraint on the energy available to the device. Hence, it is essential to make the maximum use of scarce energy to prolong the productive time of the devices. Although some miniaturized circuitry and power sources are already available, minimization of their energy consumption while meeting servo system constraints is difficult to achieve using conventional controller optimization methods. In this paper, an integer programming based optimization algorithm for such a system is discussed, specifically the prescribed rotation of the micro-robotic leg joints with minimum power and an integrated charge recovery system.

Although there are many actuation schemes available in MEMS such as thermal [1]–[3], electrostatic [4], Scratch drives with electrostatic actuation [5], [6] piezoelectric actuators often have advantages including light weight, high bandwidth, high force production and lower power consumption [7] [8].They are versatile and can be designed for producing large force over a small stroke length or large stroke length with a smaller force. By combining a number of actuators in series, a large force over a large stroke length can be achieved, the individual actuator designs borrowed from [9]

B. Edamana is with the Department of Mechanical Engineering, University of Michigan, Ann Arbor 48109 MI, USA (e-mail: bij@umich.edu).

K. Oldham is with Department of Mechanical Engineering, University of Michigan, Ann Arbor 48109 MI, USA (phone: 734-615-6327; e-mail: oldham@umich.edu).

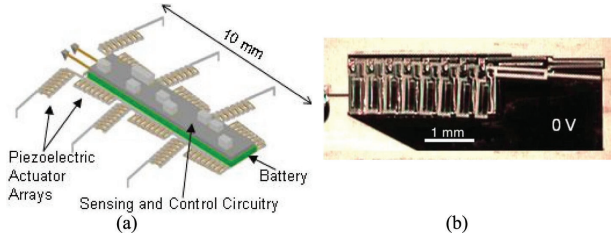

Fig. 1. (a) Concept-drawing of an autonomous micro-robot based on thin-film piezoelectric actuator joint arrays. (b) Sample Image of leg joints at 0V

used in this project can produce up to 3 degrees of more rotational motion at 20V when coupled to micro-rotating leg joints with large weight bearing capacity. They may also be combined in series to produce substantial rotation required for a micro-robotic leg joint, as in Fig. 1. Some less common electrostatic actuator designs [10] also produce comparable amounts of work to piezoelectric devices; the control strategy proposed here, targeted for capacitive loads, is applicable to such actuators as well. A major challenge in using the piezoelectric actuators for autonomous microsystems is the associated power electronics. Traditional analog amplifiers are designed to operate on resistive loads. However, the piezoelectric actuators act as a capacitor under most operating conditions. Main et al. in [11] showed that when applied to piezoelectric actuators, traditional analog amplifier based circuits consume as much as or more than 99% of energy supplied. They proposed an alternate option of using pulse-width-modulation (PWM) based switching controller circuits to compensate for these losses. This strategy reduces the energy lost in the circuit drastically, though in a switching controller, the energy used by a capacitive load is proportional to the frequency of switching. Further energy can be saved as in our previous work [12] by minimizing the number of switchings for a given motion of the actuator.

The energy savings above are made on the charging side of the actuator, but energy can be saved upon discharge as well. When voltage is applied across a piezoelectric actuator, and depending on its electromechanical coupling coefficient, a fraction of energy is used to do the mechanical work and the remainder is stored as mechanical and electrical energy. When the applied voltage is removed, the actuator returns to the original position and the stored energy is drained off. [11] and [13] showed that most of this energy can be recovered by a charge recovery circuit using a large inductor connected with storage capacitor. In this paper, this idea is converted to a partial charge recovery scheme for the use of an autonomous micro-robot where a only a small

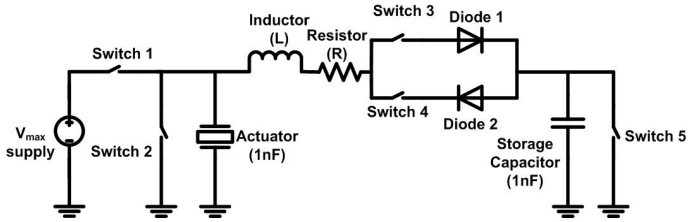

Fig. 2. The charge recovery circuit

inductor can be used. The small inductor is lighter and it allows intermediate voltage levels compared to a pure on-off controller or a full charge recovery controller. These intermediate voltage levels can be made use to span more points in the state space compared to a pure on-off controller. Because of strict energy budget and high power consumption of sensor circuits feedback is not used in this application, although the algorithm can be extended by using receding optimization horizon to incorporate feedback.

II. Dynamics of the system

A sample image of a micro-robot leg joint is given in Fig 1. The dynamics of this leg can be lumped into a mass-spring-damper system which can be represented by a second order differential equation of the form,

$$J\ddot{\theta} + b\dot{\theta} + k\theta = Gu \tag{1}$$

where J, b,and k denotes the inertia, damping and stiffness respectively and G represents the actuator gain, and u the input voltage to the actuator. This system can be represented in state space with the angle of rotation (θ) and the angular velocity ($\dot{\theta}$) of the actuator as states and this can be discretized with a sampling time T_s to obtain the following system of algebraic equations,

$$\begin{aligned} x\left((k+1)T_s\right) &= A_d x(kT_s) + B_d u(k) \\ y(kT_s) &= C_d x(kT_s) \end{aligned} \tag{2}$$

There are two important constraints on the system input. The first is that the inputs can be changed only at the sampling instants, which is addressed by appropriate choice of sampling time in discretization. The second constraint is on the values that input voltage $u(k)$ can take at each sampling instants when a charge recovery system is coupled with a switching, on-off input from the power source. These constraints are explained in the optimization section.

III. Electrical model of the system

A sample charge recovery circuit used for this study, which is derived from [13], is given in the Fig. 2. It is assumed that the storage capacitor is of same capacitance as the actuator. The 20 V supply is connected to the actuator through switch 1. The actuator can discharge itself through switch 2, or it can charge the storage capacitor when switch 3 closes. Then, the stored energy on storage capacitor can be returned to the actuator through the switch 4 or discharged to ground through the switch 5. Only one of switch 1 to 4 can be turned on at a time and switch 5 may be turned on only when switch 3 and switch 4 are in off position. Further explanation is required for the modes when either switch 3 or 4 is closed. Consider the situation when the actuator voltage is greater than the storage capacitor voltage. In order to transfer charge from the actuator to storage capacitor, switch 3 is closed. During the time that the current flows from actuator to storage capacitor, the circuit can be modeled as a second order system in terms of charges stored in actuator q_1 and storage capacitor q_2 (3). For the effective charge recovery, circuit parameters are chosen to make the system underdamped. The diode present in the circuit will prevent any reverse current and will keep the capacitor voltages constant at the overshoot points.

$$L(\ddot{q_1} - \ddot{q_2}) + R(\dot{q_1} - \dot{q_2}) + \frac{q_1 - q_2}{C/2} = V_D \tag{3}$$

where V_D is the voltage drop across the diode. Letting $q_1(0) = V_{10}C$, $q_2(0) = V_{20}C$ and the differential voltage $V = (q_1 - q_2)/C$, where V_{10} and V_{20} are the initial voltages on actuator and storage capacitor respectively.

$$\begin{aligned} L\ddot{V} + R\dot{V} + \frac{V}{C/2} &= \frac{V_D}{C} \\ V(0) &= V_{10} - V_{20} \end{aligned} \tag{4}$$

Assuming that $V_{10} > V_{20}$ before switching, then $V(t)$ will follow a step response until it reaches the maximum value and will stay there because of the diode. The response of the system up to the overshoot point then can be written as,

$$V(t) = V_D + (V(0) - V_D)e^{-\alpha t}(cos\beta t + \frac{\alpha}{\beta} sin\beta t) \tag{5}$$

where $\alpha = \frac{R}{2L}$ and $\beta = \frac{\sqrt{\frac{8L}{C} - R^2}}{2L}$. $V(t)$ reaches its maximum value when $t = \frac{\pi}{\beta}$ and the corresponding differential voltage will be the difference between the actuator voltage, V_{11}, and the storage capacitor voltage, V_{21}, after switching.

$$V_{max} = V_{11} - V_{21} = V_D - (V(0) - V_D)e^{-\frac{\alpha\pi}{\beta}} \tag{6}$$

The above equation together with the charge conservation equation $C(V_{10} + V_{20}) = C(V_{11} + V_{21})$ can be used to evaluate the actuator voltage and the storage capacitor voltage after switching:

$$V_{11} = V_D(\frac{1+\mu}{2}) + V_{10}(\frac{1-\mu}{2}) + V_{20}(\frac{1+\mu}{2}) \tag{7}$$

$$V_{21} = -V_D(\frac{1+\mu}{2}) + V_{10}(\frac{1+\mu}{2}) + V_{20}(\frac{1-\mu}{2}) \tag{8}$$

where $\mu = e^{-\frac{\alpha\pi}{\beta}}$. Using a diode with negligible voltage drop compared to the maximum voltage, the above equations can be approximated to form symmetrical equations.

$$V_{11} = V_{10}(\frac{1-\mu}{2}) + V_{20}(\frac{1+\mu}{2}) \tag{9}$$

$$V_{21} = V_{10}(\frac{1+\mu}{2}) + V_{20}(\frac{1-\mu}{2}) \tag{10}$$

These equations are derived for the case when the actuator voltage is greater than the storage capacitor voltage. If the storage capacitor voltage is higher, the charge can be returned to the actuator by closing the switch 4 (and opening switch 3) and the equations are still valid.

IV. Optimization method

A. Objective function

The objective of the optimization is to drive the states of the system θ and $\dot{\theta}$ given in Eq. 1 to a desired set of values in a prescribed time using minimum energy. Hence, the objective function is the energy used by the actuator directly from the power source. In piezoelectric actuators energy is used mainly to charge up the actuator. In the set up discussed in this paper this can be done by either the external power source or from the storage capacitor. The capacitive lose J_C is the sum of such externally powered charging or, in other words, when a transition in voltage states on the actuator occurs that is powered externally, quantified as

$$J_C = \sum_{k=1}^{n} C(u_{s_1}(k)(u(k)^2 - u(k-1)^2) + u_{s_1}(0)u(0)^2) \tag{11}$$

where C is the capacitance of the piezoelectric actuator and $u_{s_1}(k)$ is a binary variable which takes value 1 if switch 1 is on at k^{th} time instant and 0 otherwise and $u(k)$ represents the voltage on the actuator at the k^{th} instant, which can take any allowed voltage given in the automata described in the following section. In piezoelectric films with high leakage resistance, the resistive loss is negligible over short movement duration compared to the capacitive loss, and hence it is not considered in the optimization.

B. Constraints

There are three types of constraints in the optimization problem: the dynamics of the system, the final desired states and the constraints on the inputs which are explained in the following subsections.

1) System dynamics constraints: The system dynamics form pn equality constraints from (2) during optimization, as given below. Here p is the order of the system, being $p = 2$ in the case of this paper since the piezoelectric actuator is modeled as a second order system and n is the number of time steps allowed to reach the final desired states as explained in final state constraints.

$$x\left((k+1)T_s\right) \quad = \quad A_d x(kT_s) + B_d u(k) \tag{12}$$

2) Final state constraints: Since the inputs can be changed only at certain instants and can take only a certain values, it is impossible to drive the states to arbitrary points in the state space. So the aim is to reach the neighborhood of a desired final state as shown by $x(n * T_s) \in [x_d \pm \epsilon]$. This forms p inequality constraints.

3) Input transition constraints: The inputs of on-off controller can be either u_{min} or u_{max}. On the other hand, a charge recovery controller can be produce certain intermediate voltages as well. These intermediate voltages have to satisfy certain additional constraints as described below.

Case 1: A simple case is considered first. The storage capacitor discharges all its energy whenever the actuator gets charged or discharged, effectively resetting the states of the automaton. By this assumption the intermediate voltages can be predetermined. The scenario is explained in the following paragraph.

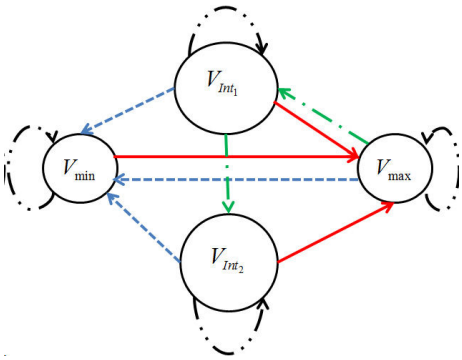

Fig. 3. The automaton showing the constraints on actuator voltage transitions for the simplest case

The actuator is charged to V_{max} when switch 1 turns on and it will either drain the charge to ground through switch 2 or it will charge the storage capacitor through switch 3. If it drains the energy the actuator voltage will go back to V_{min} and if it charges the storage capacitor the actuator voltage will reach V_{Int_1}. From V_{Int_1} the actuator can return to V_{min} or V_{max}, but the storage capacitor will drain all its energy. If the actuator recovers the charge through the switch 4, it will attain V_{Int_2}. From this state, actuator voltage may be maintained, fully charged or discharged. This results in just 4 voltage levels as shown in the automaton given in Fig. 3. The states of the automaton represents the actuator voltage at each instant of time. In order to convert these constraints to equations, a new set of binary variables v_1, v_2, v_3, v_4 are introduced, each corresponds to an input voltage in the set $V_{min}, V_{max}, V_{Int_1}, V_{Int_2}$. So the input voltage at time $t = k * T_s$ can be written as,

$$u(k) = v_1(k)V_{min} + v_2(k)V_{max} + v_3(k)V_{Int_1} + v_4(k)V_{Int_2} \tag{13}$$

and the following constraint ensures that the system is in only one state at a time (note that $v's$ are binary):

$$v_1(k) + v_2(k) + v_3(k) + v_4(k) = 1 \forall k \in 0..n \tag{14}$$

Additional constraints ensure illegal transitions such as a transition from V_{max} to V_{Int_1} do not happen. This can be done by making sure that $v_2(k)$ and $v_3(k+1)$ are not simultaneously one, as by the inequality constraint $v_2(k) + v_3(k+1) \leq 1$.

Case 2: In the second case we remove constraints on the transitions of storage capacitor voltages. This is mathematically more challenging to optimize, but it has greater potential to improve the efficiency of the system. The intermediate actuator and storage capacitor voltages are not constants in this case. The values the voltages can take at any point of time $t = (k+1)T_s$ depends on the charge stored in the actuator and storage capacitor at the previous instant $k * T_s$. At time $t = kT_s$ let the voltages on actuator and storage capacitor be V_{10} and V_{20} respectively. Then at next instant the actuator voltage can take any of the following values $\{0, 20, V_{10}[\frac{1-\mu}{2}] + V_{20}[\frac{1+\mu}{2}]\}$ and storage capacitor voltage can take any value from the set $\{0, V_{20}[\frac{1-\mu}{2}] + V_{10}[\frac{1+\mu}{2}]\}$.

The derivation of these voltages are shown in (6).

The binary variables $w_1(k)..w_7(k)$ ensure that the state in the automaton, represented in the form "(actuator voltage, storage capacitor voltage)," is one of the allowed automaton states, as shown in Fig. 4, which represents a system of allowed binary switching sequence:

$$\begin{aligned} u(k) &= w_1(k)V_{max} + w_2(k)V_{min} + \\ &\quad w_3(k)(u(k-1)[\frac{1-\mu}{2}] + u_s(k-1)[\frac{1+\mu}{2}]) + \\ &\quad w_4(k)u(k-1) + w_5(k)u(k-1) + w_6(k)V_{max} + \\ &\quad w_7 V_{min} \end{aligned} \tag{15}$$

$$\begin{aligned} u_s(k) &= w_1(k)V_{min} + w_2(k)V_{min} + \\ &\quad w_3(k)(u_s(k-1)[\frac{1-\mu}{2}] + u(k-1)[\frac{1+\mu}{2}]) + \\ &\quad w_4(k)V_{min} + w_5(k)u_s(k-1) + w_6(k)u_s(k-1) + \\ &\quad w_7 u_s(k-1) \end{aligned} \tag{16}$$

$$\sum_{i=1}^{7} w_i(k) = 1 \tag{17}$$

Here $u(k)$ and $u_s(k)$ are actuator voltage and storage capacitor voltage at time $t = k * T_S$ respectively. Some of these constraints are non-linear due to the multiplication of regular variables with binary variables. These type of constraints can be converted to a set of linear constraints by introducing a set of new variables by the following procedure [14]. Consider a new variable $z(k)$, to replace the term $w_4(k)u(k-1)$ in (15). By adding the following four additional linear constraints the above equation can be converted to a linear equation on z.

$$\begin{aligned} z(k) &\leq M w_4(k) \\ z(k) &\geq m w_4(k) \\ z(k) &\leq u(k-1) - m(1 - w_4(k)) \\ z(k) &\geq u(k-1) - M(1 - w_4(k)) \end{aligned} \tag{18}$$

where $M = max(u(k-1)) = V_{max}$ and $m = min(u(k-1)) = V_{min}$. Similarly each of the product terms are replaced by new variables and additional linear constraints are added.

The constraints on transitions of actuator voltage and storage capacitor voltages are shown in the Fig. 4. The transitions marked solid (red color) lines involve external power usage, dash-dot lines (green) employ the charge recovery circuit, dash-dot-dot (black) lines represent staying at the same state and dashed lines (blue) are discharge of either actuator or storage capacitor. From the initial optimization it was observed that the full range of possible leg motions (i.e. target final angles) can be achieved with one external powered charging of the actuator at the beginning of the motion. Thus, the problem of motion optimization may be extended to maximizing the energy stored in the storage capacitor at the end of the optimization horizon for future use.

4) Modified optimization with final storage capacitor voltage maximization: Since the external energy used for a given required rotation is the minimum possible (a single charging from the external power source) for the range of possible actuator final angles, the optimization objectives were modified to better suit repeated motions. The new objective function

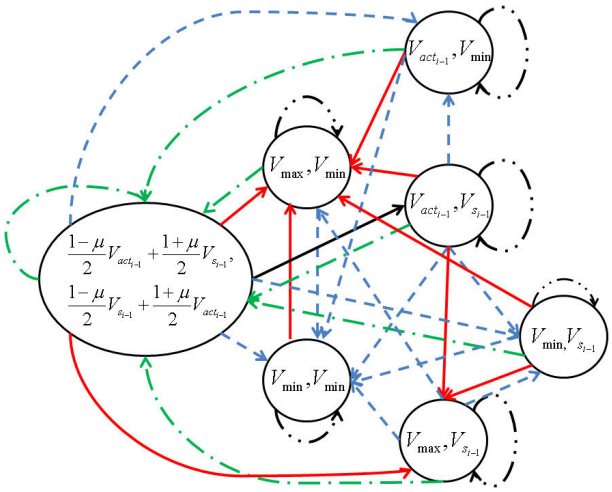

Fig. 4. Automaton showing the constraints on the input voltage for the case 2

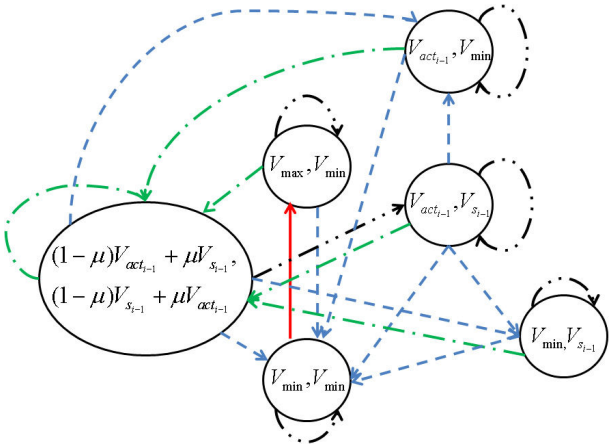

Fig. 5. Automaton showing the constraints in the modified optimization

is set to maximize the storage capacitor voltage at the end of the optimization horizon. By maximizing the final storage voltage more than one step of actuation can be achieved by one externally powered voltage switching for smaller leg motions or the additional energy required to repeat the current motion can be minimized for larger leg motions.

$$J_{modified} = u_s(n) \tag{19}$$

where n is the number of allowed time steps to reach the desired final state as given the earlier section. The minimum energy requirement of one external powered charging of actuator applied as an additional constraint. Mathematically this is done by limiting the number of transition from V_{min} to V_{max} to one (20),

$$\sum_{k=0}^{n} w_2(k)w_1(k+1) \leq 1 \tag{20}$$

This nonlinear constraint was converted to a linear one using the method shown in (18). The constraints on the modified system are shown in the new automaton given in Fig. 5.

C. Optimization solver

All three problems discussed above had linear constraints after the conversion given in (18). The first two cases had

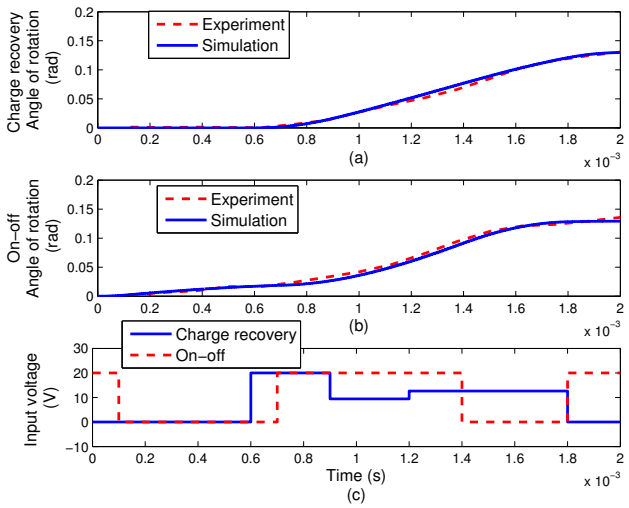

Fig. 6. (a) Micro system-Charge recovery controller response for an optimal sequence to reach 0.13rad at 2ms, (b) Micro system on-off controller response for an optimal sequence for the same state constraints (c) Optimal charge recovery controller and on-off sequences

quadratic objective functions and the third one was linear. Due to the presence of binary variable the problem is NP-hard, so the optimization needs integer programming solver. All the constraint equations and objective function were written in AMPL and solved using CPLEX. CPLEX uses branch and bound algorithm to solve integer programming problems.

V. Experimental and Simulation Results

A. Charge recovery vs. pure on-off controller

Experiments conducted on a micro-scale piezoelectric actuator with natural frequency of approximately 300 Hz is discussed here. System dynamics were identified from a step response of the system over relatively long time scales (0.015 s). Discretized the dynamics with a sampling time of 0.1 milli seconds and the control sequences were developed for a final time of 20 milli seconds. This final time allows balance between accuracy (accuracy can be improved by increasing the time horizon) and efficient speed of operation.

The MEMS actuator, the prototype robotic leg shown in Fig. 1(b), was operated using a TMS320F28335 microprocessor and Analog devices fast switches ADG5412BRUZ. Motion of the rotational joint was captured using a high speed camera at 8000 frames per second and the angle of rotation was measured using the MATLAB Image Processing Toolbox. The following second order system was identified between the input voltage and the angle of rotation of the leg in radians. Displacement angles are averaged from many different locations along the rigid portion of the leg reducing measurement error. In this case the charge recovery intermediate voltages were 9.6V and 12.4V for a 3.1nF storage capacitor and 1mH inductor.

$$\frac{y(s)}{u(s)} = \frac{1}{5.0039 \times 10^{-5}s^2 + 0.0093s + 164.6091} \quad (21)$$

After system identification, optimal on-off control sequence and optimal charge recovery sequence using the simplest

TABLE I

Micro-actuator parameters used in the dynamic intermediate charge recovery simulation study

Parameters	Values
R (Ω)	$3 * 10^9$
C (F)	$1 * 10^{-9}$
$V_{max}(V)$	20
J ($kg.m2$)	$1.4 * 10^{-12}$
b ($N.m.s/rad$)	$2.7 * 10{-}10$
k ($N.m/rad$)	$4.4 * 10{-}6$
G ($N.m/V$)	$2.8 * 10^{-8}$
$R_{Diode}(\Omega)$	2
Sampling time (T_s)(sec)	0.0001

strategy were found. Both case objectives were set to reach (0.130 ± 0.001 radians, ± 1 rad/s) at 2ms. The target final values were selected as an arbitrary step angle below the maximum displacement of the leg joint, as though instructing the leg to move a desired distance and reach zero velocity at a given time when it would be raised from or lowered to the ground in exchange with other legs on a robot. The optimal sequences were applied on a simulink model as well as on the experimental system. The experimental and simulational responses obtained from charge recovery sequence are shown in Fig. 6(a). In the simulation the final angle reaches 0.1297 radians at 2 ms, which is within the constraints given, and the experiment also follows very closely and settles around the same value. Similar behavior was also observed with the optimal on-off sequence as shown in Fig. 6(b). From the video-captured angular measurement it was verified that the actuator momentarily becomes stationary at the expected time with a displacement of 0.13 rad and less than the targeted 1 rad/s velocity. The optimal charge recovery and on-off sequences are shown in Fig. 6(c) from which it can be observed that the charge recovery sequence charges the actuator externally once compared to three times the pure on-off sequence. Hence in this example the simplest charge recovery strategy proved to be 3 times more efficient than the pure on-off controller.

In order to verify the energy consumption in the experimental switching circuitry and the MEMS actuator, current and voltage were measured while the switch is turned on charging the actuator from 0 to 20V. The energy consumption was found to be $0.27\mu J$ which is in the similar order of expected value of approximately $0.2\mu J$ for the a nominal 1 nF capacitance; additional power consumption is attributed to a combination of underestimating the true capacitance and some parasitic capacitance occurring at the actuator.This results in an experimental energy consumption per step of 0.27 μJ for the charge recovery controller and 0.81 μJ for the on-off controller in the case discussed in the last paragraph.

B. Simulational study of Multi-stage charge recovery with dynamic intermediate voltages

Dynamic intermediate voltage charge recovery could not be implemented in the experimental systems because of discrepancies in the electrical model with the experimental setup. These discrepancies arises due to high resistances in the electrical interconnects (400 Ω) and dielectric constant of

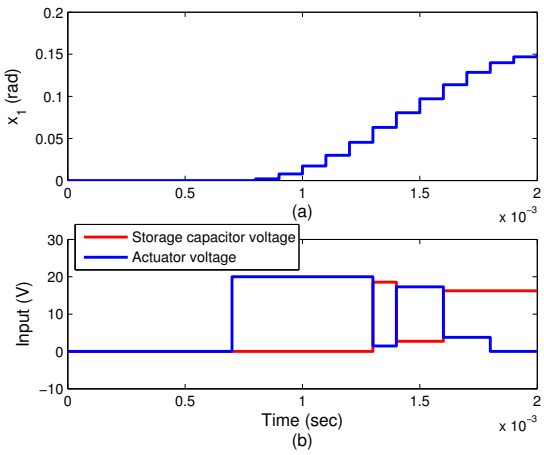

Fig. 7. Charge recovery with dynamic intermediate voltages simulation result

a thin-film piezoelectric material with applied voltage. The resistance in the interconnect can be reduced to a few Ωs by efficient interconnect routing as its planned for future designs. Nonetheless, a simulation study was conducted to explore potential advantages of multi-stage dynamic intermediate voltage charge recovery on an ideal model. From this study it was found that a wide range of angles with satisfactory accuracy could be reached by a single externally powered switching in dynamic intermediate voltage charge recovery. Hence, the objective was changed to extract more from the single power consuming switching. This is done by maximizing the final storage capacitor voltage and limiting the externally powered switching to one. The state constraints in the simulation were $x_d \in (0.14rad, 0rad/sec) \pm (0.001rad, 1rad/sec)$ at 2ms and single externally powered switching is added as a constraint, leaving the objective here as being to maximize the end storage capacitor voltage. In Fig. 7 a typical response for this scenario is given. The final storage voltage is 16.24V. So in the remaining steps this voltage together with external source can be utilized to charge the actuator. Hence, the energy consumption in future steps is only approximately 0.09 μJ per step. In terms of power, for a step frequency of 500 Hz (or 2 ms per step), this corresponds to an average power consumption of 400 μW with on-off control, 130 μW with simple charge recovery, and 90 μW with dynamic charge recovery, could the final approach be implemented.

VI. Discussion

A method for minimizing the power consumption in a MEMS piezo-electric actuator for given state constraint is presented. The main contribution of this paper is the use of partial charge recovery method making use of a smaller hence lighter inductor and the optimization of the resulting control scheme for minimizing the energy usage using integer programming. The optimization incorporated both the dynamics of the actuator as well as circuitry constraints. The integer programming problem is solved by using CPLEX solver. Since the primary objective was to have a controller with a minimum energy consumption the high energy consumption of integrated MEMS sensors (compared to actuation power levels) are avoided and hence the results in this paper are shown for open loop scenarios. In these scenarios, significant robustness is given away for having minimum possible energy consumption and the controller performance entirely depends on how accurately the system can be identified. We note, however, that the method discussed here can be extended to incorporate feedback by using model predictive control technique. The model predictive control technique employs a receding horizon optimization applying only the first input of each optimization.

VII. Acknowledgements

The authors thank the Army Research Laboratory and the Lurie Nanofabrication Facility for their support in prototype robot fabrication, as well as the National Science Foundation, grant #0954422 for its support.

References

[1] M. Mohhebi, M. Terry, K. Bhringer, G. Kovacs, and J. Suh, "Omnidirectional walking microrobot realized by thermal microactuator arrays," *proceedings of 2001 ASME International Mechanical Engineering Congress, New York, NY, USA*, pp. 1–7, 2001.

[2] A. Bonvilain and N. Chaillet, "Microfabricated thermally actuated microrobots," *proceedings of 2003 IEEE International Conference on Robotics and Automation, Taipei, Taiwan*, pp. 2960–2965, 2003.

[3] T. M. Ebefors, U. Johan, E. Klvesten, and G. Stemme, "A walking silicon micro-robot," *proceedings of 10th International Conference on Solid-State Sensors and Actuators, Sendai, Japan*, pp. 1202–1205, 1999.

[4] S. Hollar, A. Flynn, C. Bellow, and K. Pister, "Solar powered 10 mg silicon robot," *proceedings of MEMS 2003, Kyoto, Japan*, pp. 706–711, 2003.

[5] R. Linderman and V. Bright, "Nanometer precision positioning robots utilizing optimized scratch drive actuators," *Sensors and Actuators A: Physical*, vol. A91, no. 3, pp. 292–300, July 2001.

[6] B. Donald, G. Levy, C. McGray, I. Papotry, and D. Rus, "An untethered electrostatic, globally controllable mems micro-robot," *Journal of Microelectromechanical Systems*, vol. 15, no. 1, pp. 1–15, February 2006.

[7] E. Steltz, M. Seeman, S. Avadhanula, and R. S. Fearing, "Power electronics design choice for piezoelectric microrobots," *IEEE/RSJ Int. Conf. on Intelligent Robots and Systems*, pp. 1322 – 1328, 2006.

[8] M. Sitti, "Piezoelectrically actuated four-bar mechanism with two flexible links for micromechanical insect thorax," *IEEE/ASME Transactions on Mechatronics*, vol. 8, no. 1, pp. 26–36, March 2003.

[9] K. Oldham, J. Pulskamp, R. Polcawich, and M. Dubey, "Thin-film pzt actuators with extended stroke," *Journal of Microelectromechanical Systems*, vol. 17, no. 4, pp. 890–899, August 2008.

[10] E. Sarajlic, E. Berenschot, N. Tas, H. Fujita, G. Krijnen, and M. Elwenspoek, "Fabrication and characterization of an electrostatic contraction beams micromotor," *In Proceedings of the 19th IEEE International Conference on Micro Electro Mechanical Systems (MEMS), Istanbul, Turkey*, pp. 814–817, January 2006.

[11] J. Main, D. Newton, L. Massengill, and E. Garcia, "Efficient power amplifiers for piezoelectric applications," *Smart Materials and Structures*, vol. 5, no. 3, pp. 766–775, August 1996.

[12] B. Edamana, B. Hahn, J. S. Pulskamp, R. G. Polcawich, and K. Oldham, "Modeling and optimal low-power on-off control of thin-film piezoelectric rotational actuators," *Accepted for publishing in IEEE/ASME Transactions on mechatronics*, 2010.

[13] D. Campolo, M. Sitti, and R. S. Fearing, "Efficient charge recovery method for driving piezoelectric actuators with quasi-square waves," *IEEE Transaction on Ultrasonics, Ferroelectrics, and Frequecy Control*, vol. 50, no. 3, pp. 237–244, March 2003.

[14] A. Bemporad and N. Girogetti, "A sat-based hybrid solver for optimal control of hybrid systems," *Lecture Notes in Computer Science*, vol. 2993, pp. 126–141, 2004.